



LAWRENCE  
LIVERMORE  
NATIONAL  
LABORATORY

# Concept Development for Astrophysically Relevant Turbulence on NIF

R. P. Drake

December 20, 2012

## **Disclaimer**

---

This document was prepared as an account of work sponsored by an agency of the United States government. Neither the United States government nor Lawrence Livermore National Security, LLC, nor any of their employees makes any warranty, expressed or implied, or assumes any legal liability or responsibility for the accuracy, completeness, or usefulness of any information, apparatus, product, or process disclosed, or represents that its use would not infringe privately owned rights. Reference herein to any specific commercial product, process, or service by trade name, trademark, manufacturer, or otherwise does not necessarily constitute or imply its endorsement, recommendation, or favoring by the United States government or Lawrence Livermore National Security, LLC. The views and opinions of authors expressed herein do not necessarily state or reflect those of the United States government or Lawrence Livermore National Security, LLC, and shall not be used for advertising or product endorsement purposes.

This work performed under the auspices of the U.S. Department of Energy by Lawrence Livermore National Laboratory under Contract DE-AC52-07NA27344.

## **Final Report**

### **Concept Development for Astrophysically Relevant Turbulence on NIF**

Subcontract No. B598242

Principal Investigator: R Paul Drake

Department of Atmospheric, Oceanic and Space Sciences, University of Michigan, Ann Arbor, Michigan 48109, USA

(a) Abstract: We carried out the research proposed in the proposal and developed a specific concept for the generation of fully developed Rayleigh-Taylor turbulence on NIF.

(b) Objectives: The only objective was to develop a specific concept for the generation of fully developed Rayleigh-Taylor turbulence on NIF. See below.

(c) No publications have yet been produced.

(d) Other relevant information follows.

Under this contract we carried out the design study that we proposed. We demonstrated that NIF is capable of producing self-similar turbulence resulting from the Rayleigh-Taylor instability. Our detailed study shows that NIF can in fact produce a more-developed turbulent state than we estimated in the proposal. Thus, NIF can go far beyond any previous experiment in the generation of a hydrodynamic state that can be described as fully developed turbulence.

To accomplish our study, we first assessed what sort of experimental system NIF was capable of driving, for modest values of the laser parameters. We developed a design for a specific target that could produce Rayleigh-Taylor turbulence. We then performed hydrodynamic simulations of this system. We analyzed the results of these simulations to determine the likely evolution of the turbulence in a NIF experiment.

The results of our work are discussed in the following, which is a draft paper for publication. We are now undertaking multidimensional simulations, which will also be included in the paper before it is submitted.

# A preliminary design of a two-dimensional Rayleigh-Taylor experiment on NIF

## Abstract

An preliminary design of an experiment meant to investigate the evolution of multimode Rayleigh-Taylor instability (RT) is presented. This experiment is intended to provide a direct measurement of the two-dimensional bubble front evolution in the hydrodynamic regime. RT growth for the proposed design has been analyzed using one-dimensional direct numerical simulations in HYADES, and a self-similar behavior model. The proposed design assures a significant bubble merging process ( $\sim 3$ -4 bubble merger generations), bringing the bubble front to the self-similar stage. The design takes advantage of the National Ignition Facility (NIF) capabilities to provide a large enough laser spot area ( $\sim 0.5$ -1 cm<sup>2</sup>), along with a low enough drive, so preheat effects remain reasonably small.

## 1 Introduction

The Rayleigh-Taylor (RT) instability [24, 25] occurs when a light fluid accelerates a heavier fluid (or where a pressure gradient opposes a density gradient). This instability is of high importance in designing Inertial Confinement Fusion (ICF) capsules [11, 15, 23] and in understanding many astrophysical phenomena [3, 12, 21, 6, 19]. Under unstable conditions (i.e. when  $\nabla P \cdot \nabla \rho < 0$ , where  $P$  is pressure and  $\rho$  is density), small perturbations on the interface between the fluids grow into bubbles of light fluid penetrating the heavy fluid and spikes of heavy fluid penetrating the light fluid, eventually creating a turbulent mixing zone (TMZ). Our interest in the current work is in the very late-time TMZ evolution.

In the simple case of a periodic single-mode initial perturbation, the flow is governed by the single bubble evolution. When the amplitude to wavelength ratio is small (i.e.  $a/\lambda \ll 1$ ), the perturbation grows exponentially in time:

$$a(t) = a_0 \cdot e^{\gamma t} \quad (1)$$

where  $\gamma = \sqrt{Akg}$ ,  $k = 2\pi/\lambda$  is the mode number and  $A$  is the Atwood number [24]. When the perturbation continues its growth, and the ratio  $a/\lambda$  reaches the value of  $\sim 0.1$ , harmonics of high-order develop [27, 28], and the linear solution presented in Eq. (1) is no longer valid. For  $A \neq 0$  these nonlinear harmonics results with asymmetries between the bubble and the spike in second order. In the third order, they result in a velocity reduction due to the inertial drag force acting on the bubble and spike. At very late times, the perturbation growth rate reaches an asymptotic value, and bubbles and spikes grow with a constant growth rate of  $u_{b,s} = \sqrt{2A/(1 \pm A)} \cdot g\lambda/C_d$  [13], where the plus and minus signs are for bubbles and spikes, respectively, and  $C_d$  is a drag coefficient, equal to  $2\pi$  for two-dimensional geometry.

When the initial perturbation is a multimode one, the TMZ evolution differs from the simple single-mode case. The flow is governed by an inverse cascade

process (i.e. bubble competition), and larger and larger structures are continually generated [9]. In the bubble competition process, large bubbles overtake the volume originally occupied by smaller bubbles. Due to this mechanism, the average wavelength  $\langle\lambda\rangle$  of the multimode perturbed interface increases with time and the width of the overall perturbation grows faster than in the case of a single-mode interface. Alon et al. [1, 2] presented a statistical bubble competition model to study the temporal evolution of the multimode RT instability front, addressing it as a two-dimensional array of rising bubbles, moving in their single-mode asymptotic velocity and competing with their smaller neighbors. It was found, that after  $\sim 3$  merging generations the large-scale structure in the mixed region (i.e. the bubble front size distribution) reaches a self-similar behavior (a generation is defined as a factor of 2 increase of the average wavelength). In this regime the initial conditions are forgotten, and the amplitude temporal evolution of the RT bubble front is:

$$h_b = \alpha_b A g t^2 \quad (2)$$

with  $\alpha \approx 0.05$ . Similar results were found in numerical studies [26, 5]. The RT spike front was found to exhibit similar behavior,  $h_s = \alpha_s A g t^2$ , where  $\alpha_s = f(A)$ , where  $f(A)$  is a specific function of Atwood number. The ratio between the bubble front average height and average wavelength was found to depend on the Atwood number,  $h_b/\langle\lambda\rangle = b(A)$ , having:

$$b(A) \approx \frac{1}{2(1 + |A|)} \quad (3)$$

The Alon et al. model was later expanded to three dimensional geometry by Oron et al. [20]. The three dimensional model predictions were compared to the Linear Electric Motor (LEM) experimental results presented by Dimonte & Schneider [4], with good agreement for the scaling parameters  $\alpha_{b,s}$  and  $h_b/\langle\lambda\rangle$ . However, the experiments did not provide a direct measurement of the bubble front size distribution due to their 3D nature, and the models validity in this manner was not confirmed. Hence, we will try to establish an experimental platform, in which the 2D, multimode RT instability evolution can be measured directly, having a large enough number of bubble generations. In specific, we focus on driving a system having the maximum possible RT growth on NIF. This will be done using one-dimensional HYADES simulations for predicting the typical time scales and possible acceleration and Atwood numbers profiles, and then evaluating the RT growth assuming self similar behavior.

The potential of NIF to do fundamental hydrodynamic experiments requires a design that best exploits the available energy and potential diagnostics. The use of NIF as the drive platform in this design holds the benefit of obtaining a ratio of target width to the average initial wavelength of  $L/\langle\lambda_0\rangle \gtrsim 100$  and a linear RT growth factor of  $\sim 100$ . Both of these would be substantial advances in the state of the art.

The 2D case which is the primary focus here offers the advantage that one can very cleanly diagnose the 2D structure. However, 3D effects will eventually

disrupt this structure and will put a limit on how far a 2D system can evolve as such. The experiment design discussed here can be used with 3D initial conditions to explore the evolution of 3D RT turbulence. In this case, it will be diagnostic resolution that determines the degree to which one can examine the spectrum of modulations. Ultimately, the thickness of the x-ray sheet that can produce good signal to identify the interface will determine the smallest 3D features one can distinguish and the range of bubble sizes one can sample in a statistically meaningful way.

## 2 Basic considerations

Here we present the basic considerations for the experiment. We start with a description of the laser platform parameters and requirements, and then describe the target composition and dimensions.

In order to have obtain a measurement of the bubble front shape and spectrum, we consider an open planar geometry where the system can evolve without the hydrodynamic or diagnostic consequences of stagnation events or geometrical artifacts. Also, we focus on a blast wave RT driven design, as was done in some past studies [21, 14]. In order to achieve that, one must have:

- A large enough time scale to allow several merging generations.
- Negligible effects of radiative preheat from the laser corona upon the perturbed interface. The radiative preheat caused by x-rays emitted from the ablating material [8] can change the hydrodynamic nature of the flow. This effect is modeled in the 1D simulations presented in section 3 and is suppressed by a thermal insulator composed of brominated plastic, discussed below.
- Negligible effects of electron preheat. The electrons in the thermal distribution produced in this general class of experiments cannot penetrate through many microns of plastic material and have no ability to affect the interface of interest. However, in general laser-target experiments can produce suprathermal distributions of electrons by means of laser-plasma instabilities and such electrons, or the x-rays they emit, can in principle perturb an embedded interface of interest. In the experimental design presented here, we minimize the potential for this by keeping the laser irradiance below the upper limit of  $\sim 10^3$  TW/cm<sup>2</sup>.
- Insignificant additional two and three dimensional effects. An example of such an effect is the rarefaction that moves radially inward from the outer boundary of the laser-driven, high-pressure plasma. This requires that the laser drive spot size should be large enough so information moving radially inward from will not significantly influence the phenomena of interest within an interior volume that can be diagnosed. We discuss this in section 4.

In experiments of this type, the laser has two purposes. First, it must drive the hydrodynamics of interest and second, the laser must provide the diagnostic energy. This leads to the use of a laser pulse of several ns, with a total experimental time scale of tens of ns. The diagnostic approach of interest here is imaging x-ray Thomson scattering (XRTS), which can create a sheet of x-rays and to detect material interfaces by the difference in scattered intensity across these interfaces. This will enable measurement of structure on an interface along a slice through an experiment, just as do laser induced fluorescence and particle image velocimetry. The diagnostic system is described in detail for NIF parameters in [10], and will not be discussed in the present work.

For evaluating the possible experimental regimes, we make several assumptions about NIF,s:

- NIF can operate at  $\sim 700$  kJ for these experiments, with 350 kJ able to irradiate the planar surface of interest. (The other 350 kJ are available for the diagnostic.)
- the pulse length will be  $\lesssim 3$  ns. For the specific design discussed here, we use a pulse length of 2 ns.
- the available Distributed Phase Plates (DPPs) will allow one to overlap half the NIF beams (96) to obtain an adequately uniform spot several mm in diameter

These specific numbers correspond to a total power of 175 TW. If, for example, one uses a 4 mm diameter of the irradiated spot,  $L$ , produced by overlapping the 96 beams, one obtains an irradiance of  $\sim 350$  TW/cm<sup>2</sup>. This irradiance is low enough to avoid significant preheat by fast, superthermal electrons. In addition, if the typical initial wavelength of the perturbations is  $\langle \lambda_0 = \sim 50 \mu\text{m}$ , we get  $L/\langle \lambda_0 \rangle \approx 80$ .

A schematic description of the target is presented in Fig. 1. The first layer is a polycarbonate ablator, with a density of 1.2 g/cm<sup>3</sup> and length of 100  $\mu\text{m}$ . This length is required to ensure that the ablator is not consumed by the ablation front created on the ablator face, so no interaction between the laser and the target inner layers will occur. Following the concept presented in Glendinning et al. [8], the second layer is made from another 100  $\mu\text{m}$  thick brominated polystyrene ( $C_{50}H_{48}Br_2$ ), with a density of 1.2 g/cm<sup>3</sup>. This layer is needed in order to prevent x-ray pre-heat effects on the material interfaces of the target, so that the interface stays sharp. Interface broadening by preheat may inhibit the RT growth, decrease the blast wave velocity or cause significant changes in the initial condition. Note that both layers lengths were optimized using radiation-hydrodynamic simulations for the specific experimental design, described below. The third layer consists of a 2500  $\mu\text{m}$  thick low-density (0.1 g/cm<sup>3</sup>) carbon foam (CRF). This layer is used as the low density material for the RT evolution, and has to be long enough to prevent information returning from its back side during the experimental time frame. Note that because the target thickness is smaller than the irradiated spot, one expects the shock wave and interface to remain planar during this experiment. This is discussed further below.

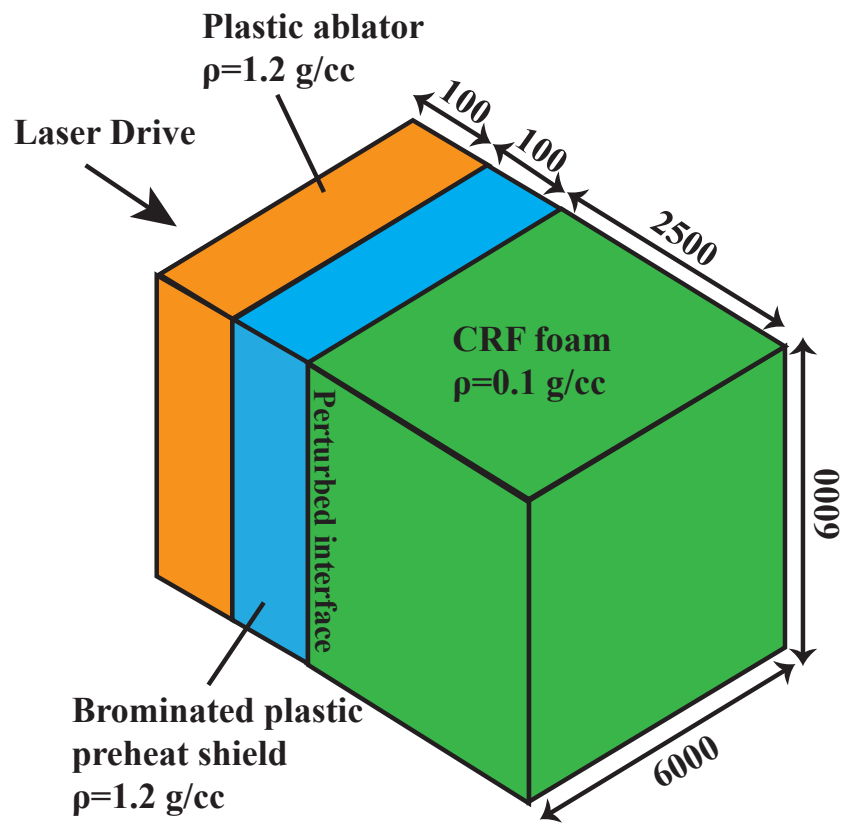


Figure 1: (color) Schematic description of the proposed target, not to scale. Dimensions are given in  $\mu\text{m}$ .

### 3 One-dimensional dynamics

In order to evaluate the possible one-dimensional time scales and RT relevant properties, one-dimensional simulations were conducted with the HYADES code [16]. HYADES is a Lagrangian hydrodynamic code with multigroup-diffusion radiation transport, single-group, flux-limited diffusive electron heat transport, a laser absorption calculation, and average-atom ionization, tracking total mass density and momentum density and independently solving for the electron and ion temperatures. The simulation used a SESAME equation of state for CH. Three laser drive irradiance values were considered for the one-dimensional simulations - 100, 250 and 500 TW/cm<sup>2</sup>. This spans the range likely to be of interest for the experiment. We note that the irradiance used in 1D simulations typically must be reduced by some factor of order 30% to match experiments. As a result, the simulations at 250 TW/cm<sup>2</sup> likely correspond to what one might observe at the nominal value of 350 TW/cm<sup>2</sup> discussed above.

Density and electron temperature contour maps in the X-t plane are presented in Fig 2 for all three laser irradiance values. It can be seen in Fig 2a-c that the laser energy deposition launches a shock wave into the ablator, followed by an ablation front. When the laser pulse ends at 2 ns, the shock wave turns into a blast wave, transmitted into the CRF foam at  $t \approx 5.5, 4$  and  $3.1$  ns for the laser irradiances of 100, 250 and 500 TW/cm<sup>2</sup>, respectively. The RT unstable interface (preheat shield/CRF interface, marked with solid black lines in the figures) is initially accelerated to some initial velocity (different for each irradiance) and then decelerates, according to the blast wave profile. It can be seen that the initial RT interface velocity and the following deceleration increase with laser irradiance. When examining Fig. 2d-f, one can see that the temperatures inside the preheat shield and the CRF increase with laser irradiance as well. The preheat effect (i.e. RT interface movement prior to the blast wave passages) is negligible for the irradiances of 100 and 250 TW/cm<sup>2</sup>. In the 500 TW/cm<sup>2</sup> case (Fig 2c), the interface moves  $\sim 5 \mu\text{m}$  prior to the blast wave arrival.

In Fig. 3 the one-dimensional profiles from the 250 TW/cm<sup>2</sup> simulation of the density, pressure, velocity and electron temperature ( $\log_{10}$  scale) are shown for  $t=10, 20$  and  $30$  ns. A typical blast wave shape is evident on the density, pressure and velocity profiles, with densities and pressures of  $0.5\text{-}1.0 \text{ g/cm}^3$  and  $1\text{-}2 \text{ Mb}$ . A sharp density jump on the interface between the preheat shield and the CRF is evident for all times. The temperature in the unshocked material is relatively low at all three times, approximately  $6 \cdot 10^{-5} \text{ keV}$ , indicating that radiative pre-heat remains small.

In Fig. 4 the Atwood number, acceleration, and velocity of the interface are presented as a function of time. Also shown is the position of the interface (Fig. 4d). The predicted post blast wave passage Atwood number is  $\sim -0.5$  (Fig 4a). By examining the acceleration profile (Fig. 4b-c), we can see that the blast wave front accelerates the interface to peak values of  $\sim 30, 50$  and  $70 \mu\text{m/ns}$  for 100, 250 and 500 TW/cm<sup>2</sup> laser irradiance, respectively. Immediately after that, the interface starts to decelerate in a decaying fashion. Since the Atwood number

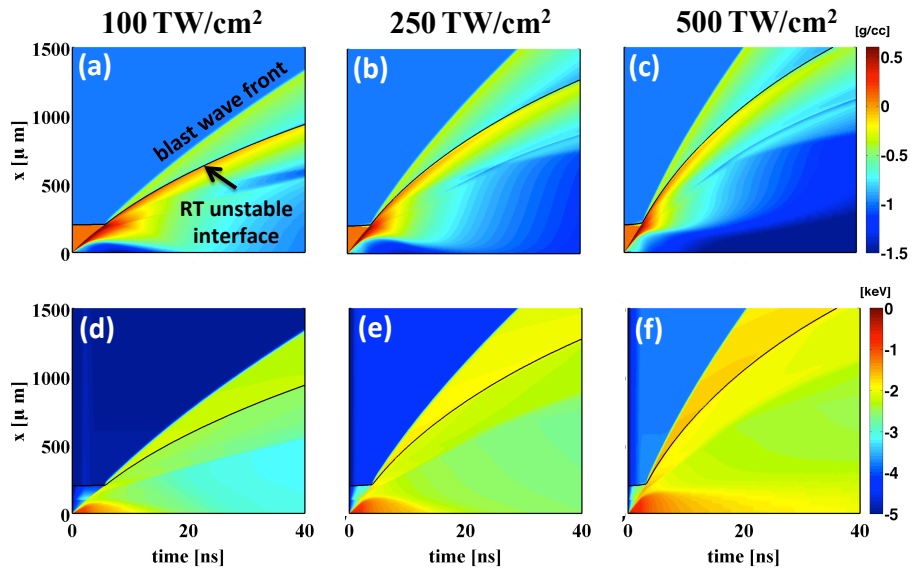


Figure 2: X-t contour map of  $\log_{10}(\rho)$  (a-c) and  $\log_{10}(T_i)$  (d-f) from the one-dimensional simulations performed with laser irradiance of 100, 250 and 500 TW/cm<sup>2</sup>. Solid black lines represent the brominated preheat shield and CRF foam interface position. Here  $t=0$  and  $x=0$  represent the laser drive initiation time and the initial laser-driven-surface location, respectively.

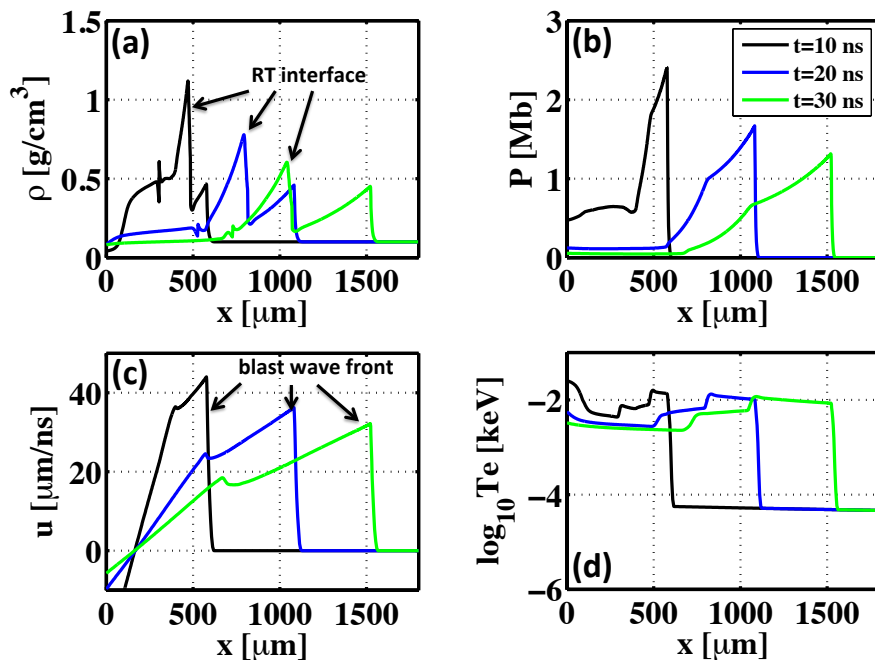


Figure 3: (color) One-dimensional profiles of the density (a), pressure (b), velocity (c) and  $\log_{10}$  of electron temperature (d) from the one-dimensional simulation with laser irradiance of  $250 \text{ TW/cm}^2$ , at  $t=10, 20$  and  $30 \text{ ns}$ .

is negative at all times, the transition from positive to negative acceleration marks the beginning of the RT unstable regime. For all three simulations, the deceleration converges to zero at  $\sim 40 \text{ ns}$ . Therefore, we mark this time ( $40 \text{ ns}$ ) as the experimental time scale. Note that the impulsive positive acceleration of the interface by the blast wave front induce some Richtmyer-Meshkov instability (RM) growth [17, 22], which can be viewed as adding to the total growth or as establishing an initial condition for RT with a significant velocity perturbation [18, 7]. However, the RM contribution is expected to be small comparing to the RT growth, due to the fast decay in the induced velocity behind the blast wave front.

## 4 Estimation of RT growth

In order to estimate the expected RT growth, we used the one-dimensional simulations presented in section 3. Since the perturbation evolution is proportional to the distance traveled by the interface, we start by examining the interface dynamics in this sense. The overall distance  $D_{tot}$  travelled by the interface is:

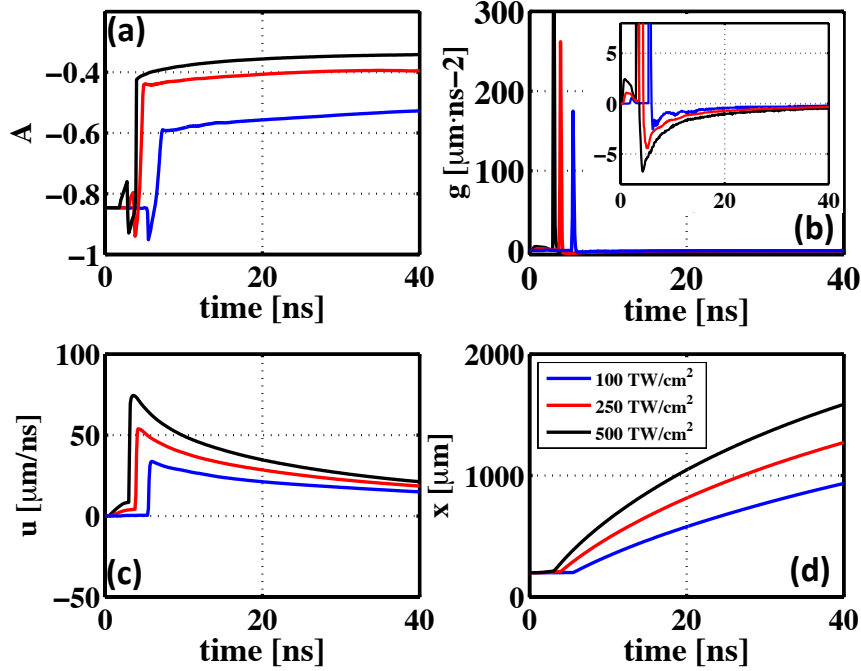


Figure 4: (color) RT relevant properties as a function of time on the unstable interface (a-c) and interface position (d), extracted from the one-dimensional simulation. (a) - Atwood number. (b) - acceleration profile. (c) - velocity profile. (d)- interface position.  $t=0$  represents the laser drive initiation time.

$$D_{tot} = x_0 + u_0 t + D_{RT} \quad (4)$$

Where  $x_0$  is simply the initial interface position, equal to  $200 \mu\text{m}$ ,  $u_0$  is the initial velocity induced on the interface by the passing blast wave, and the last term in the right hand side is the RT contribution:

$$D_{RT} = \iint (g(t) dt) \quad (5)$$

For this term, we take only the negative values of  $g$ , meaning  $g(t) = \min[g(t), 0]$ . It is an important point about these blast-wave-driven systems that it is  $D_{RT}$ , and not the total interface displacement  $D_{tot}$ , that determines the RT growth. In Fig. 5, the initial interface velocity and the different contributions calculated using Eq. 4  $\mu\text{m}$  are presented for  $t=40$  ns. It can be seen, that  $D_{RT}$  is  $-420$ ,  $-880$  and  $-1380 \mu\text{m}$  for the cases of  $100$ ,  $250$  and  $500 \text{ TW/cm}^2$ , respectively. Defining an average acceleration as  $\langle g \rangle = 2D_{RT}/t^2$ , and taking  $t=40$  ns, we get that  $\langle g \rangle = -0.7$ ,  $-1.35$  and  $-2.1 \mu\text{m/ns}$  for the  $100$ ,  $250$  and  $500 \text{ TW/cm}^2$  cases.

Repeating the same calculation for the first 10 ns, we get higher values, having  $\langle g \rangle = -1.4, -2.7$  and  $-4 \mu\text{m}/\text{ns}$

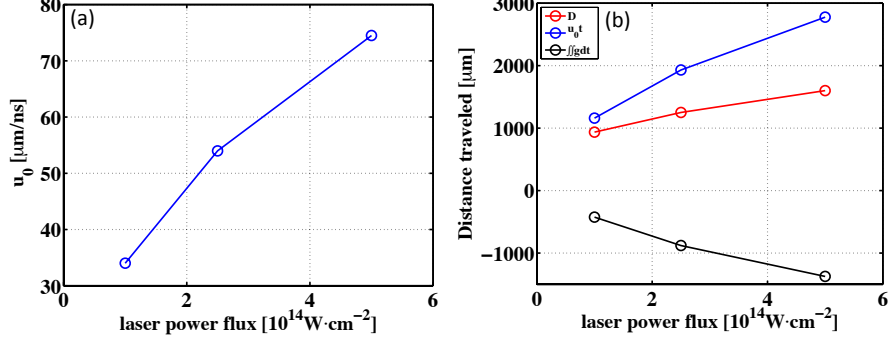


Figure 5: (color) (a) the initial interface velocity  $u_0$  and (b) the total distance travelled (red), the distance contribution of the initial interface velocity  $u_0 t$  (blue), and the RT contribution  $D_{RT}$  (black), all given for  $t=40$  ns.

If  $a_0/\langle\lambda_0\rangle \ll 1$ , the perturbations initially grow exponentially, according to the linear solution (Eq. 1). This phase ends when  $a/\langle\lambda\rangle \approx 0.1$ . The ending time of the linear growth phase for each laser irradiance,  $t_{asy}$  can be estimated simply by:

$$t_{asy} \approx \frac{\log(0.1\langle\lambda_0\rangle)}{a_0\sqrt{Ak\langle g \rangle}} \quad (6)$$

Assuming that  $a_0/\langle\lambda_0\rangle \approx 0.03$  and  $\langle\lambda_0\rangle \approx 50 \mu\text{m}$  we get  $t_{asy} \lesssim 3$  ns. Since the linear phase of the RT growth is short comparing to the overall 40 ns time scale of the experiment, we assume that the growth is self similar at all times, and generalize the Alon et al. [2] relation (Eq. 2) for the increase in bubble front height:

$$h_b - h_{b,0} = 2\alpha_b A \iint g(t) dt \quad (7)$$

Applying Eq. 7, the expected RT amplitude can be derived. Substituting Eq. 3 into Eq. 7 yields the increase in average wavelength:

$$\langle\lambda\rangle - \langle\lambda_0\rangle = \frac{2\alpha_b A}{b(A)} \iint g(t) dt \quad (8)$$

Where  $b(A) \approx 1/3$  for the Atwood numbers at hand ( $|A| \approx 0.5$ , see Fig 4a). In Fig. 6, solutions of Eq. 7 and Eq. 8 are plotted for all three laser irradiances. As expected, the increase in  $h_b$  and  $\langle\lambda\rangle$  becomes larger as the irradiance increases.

Since  $\langle\lambda\rangle \sim t^2$ , the ratio between the times of the  $n$  and  $n+1$  merging generations is  $t(n+1)/t(n) \approx \sqrt{2}$ . Using Eq. 8, this yields a simple relation for the total number of generations  $N_g$ :

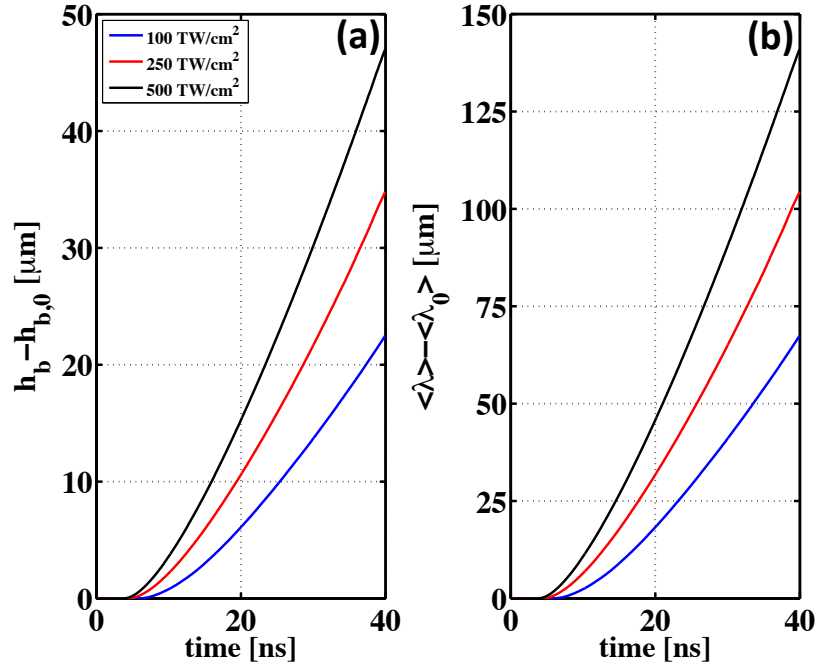


Figure 6: (color) (a) increase in bubble front height (Eq. 7) and (b) increase in average wavelength (Eq. 8).

$$N_g \approx \log_2 \frac{\langle \lambda_0 \rangle + \frac{2\alpha_b A}{b(A)} \iint g(t) dt}{\langle \lambda_0 \rangle} \quad (9)$$

The predicted number of generations for the three laser irradiances is presented in Fig 7. It can be seen that one can get  $\sim 2 - 3$  merging generations for  $\langle \lambda_0 \rangle \approx 20 \mu\text{m}$ , and  $\sim 3 - 4$  merging generations for  $\langle \lambda_0 \rangle \approx 10 \mu\text{m}$ . The expected wavelength at  $t=40 \text{ ns}$  is  $\sim 160 \mu\text{m}$ , for both initial wavelengths.

As was mentioned in section 1, it is essential that the region of interest on the interface remain planar and undisturbed by effects other than the axial acceleration. This implies that signals from the lateral edges of the experiment must not propagate too far inward during the period of interest. These signals develop in the form of rarefactions that travel inward as material expands outward, moving perpendicular to the blast wave toward the target center. Where these rarefactions interact with the TMZ, they change the one-dimensional RT conditions on the surface (i.e. Atwood number and acceleration profile).

Since the rarefaction moves at the speed of sound of the shocked material, we can use the simple ideal gas relation to estimate the sound speed,  $c = \sqrt{(\gamma P/\rho)}$ , from the simulations discussed above. Assuming  $\gamma=5/3$ , we find  $c \approx 25 \mu\text{m/ns}$  for the typical values from the one-dimensional simulations of

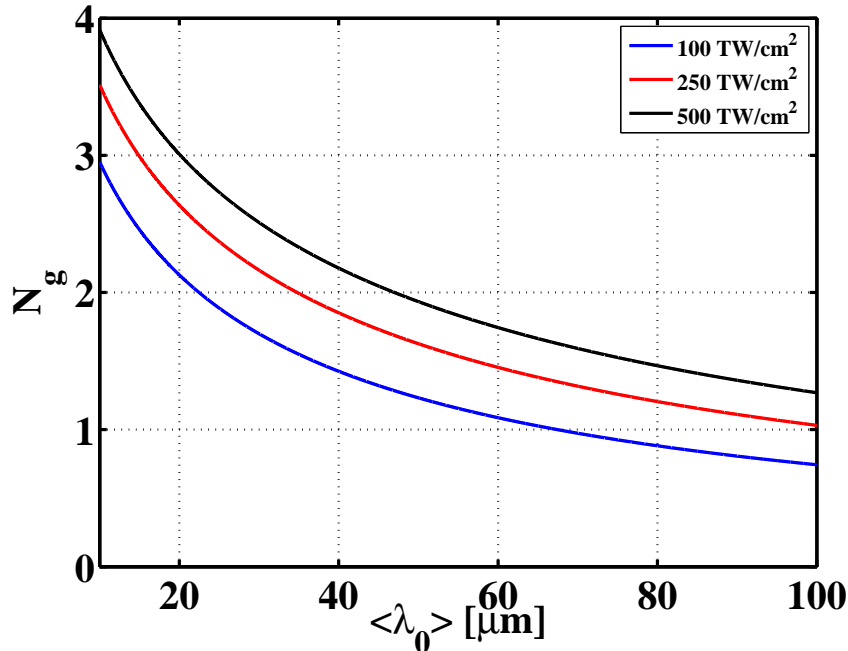


Figure 7: (color) Predicted number of merging generations expected for the different laser irradiances.

the shocked ablator and CRF. Therefore we estimate the rarefaction region of influence by assuming that the target is cylindrical, so that the rarefaction depth  $R_r$  at any time  $t$  is determined by  $R_r = ct$ . The unaffected region will then be a cylinder with a diameter  $D$ , equal to  $L - 2ct$ , where  $L \approx 8 \cdot 10^3 \mu\text{m}$  is the target width, equal to the laser spot size diameter. With total time  $t \sim 40$  ns we find  $D \approx 8 \cdot 10^3 - 2 \cdot 25 \cdot 40 \approx 6 \cdot 10^3 \mu\text{m}$ . Assuming maximal wavelengths of  $200 \mu\text{m}$ , the minimal expected number of bubbles in the unaffected region is  $\sim 30$ , large enough to allow a statistical analysis.

## 5 Summary

The feasibility of a multimode RT experiment on NIF was analyzed using one-dimensional simulations, combined with simple estimates of RT evolution based on self-similar analysis. The proposed experiment is based on a blast wave driven design. It was found, that driving a planar system having an Atwood number of  $\sim 1/2$  to  $\sim 3$ -4 merging generations is possible, using an initial average wavelength of  $\sim 10 \mu\text{m}$ , a spot size radius of  $\sim 4 \cdot 10^3 \mu\text{m}$ , and a 2 ns pulse length. The experimental time scale for the specific design is  $\sim 40$  ns. Under these conditions, the bubble front evolution is expected to develop a self-similar

evolution.

The expected amplitude is  $\sim 50 \mu\text{m}$ . The overall translation of the interface is expected to be  $\sim 1500 \mu\text{m}$ , with typical deceleration average values of 1-2  $\mu\text{m}/\text{ns}$ , resulting with an effective RT breaking distance ( $D_{RT}$  above) of  $\sim -1000 \mu\text{m}$ .

It was also found, that for realistic experimental parameters the expected width of the region that is not affected by the rarefaction is  $\sim 6 \cdot 10^3 \mu\text{m}$ , allowing an adequate diagnostic view of an unperturbed interface.

## ACKNOWLEDGMENTS

This work was funded primarily by the Lawrence Livermore National Laboratory under Subcontract B598242. Additional support was provided by the NNSA-DS and SC-OFES Joint Program in High-Energy-Density Laboratory Plasmas, grant number DE-FG52-09NA29548, the National Laser User Facility Program, grant number DE-NA0000850, and the Predictive Sciences Academic Alliances Program in NNSA-ASC via grant DEFC52-08NA28616.

## References

## References

- [1] U. Alon, J. Hecht, D. Mukamel, and D. Shvarts. Scale invariant mixing rates of hydrodynamically unstable interfaces. *Physical review letters*, 72(18):2867, 1994.
- [2] U. Alon, J. Hecht, D. Ofer, and D. Shvarts. Power laws and similarity of rayleigh-taylor and richtmyer-meshkov mixing fronts at all density ratios. *Physical review letters*, 74(4):534–537, 1995.
- [3] D. Arnett, B. Fryxell, and E. Mueller. Instabilities and nonradial motion in sn 1987a. *The Astrophysical Journal*, 341:L63–L66, 1989.
- [4] G. Dimonte and M. Schneider. Density ratio dependence of rayleigh–taylor mixing for sustained and impulsive acceleration histories. *Physics of Fluids*, 12:304, 2000.
- [5] G. Dimonte, DL Youngs, A. Dimits, S. Weber, M. Marinak, S. Wunsch, C. Garasi, A. Robinson, MJ Andrews, P. Ramaprabhu, et al. A comparative study of the turbulent rayleigh–taylor instability using high-resolution three-dimensional numerical simulations: the alpha-group collaboration. *Physics of Fluids*, 16:1668, 2004.
- [6] R.P. Drake. Hydrodynamic instabilities in astrophysics and in laboratory high-energy–density systems. *Plasma physics and controlled fusion*, 47(12B):B419, 2005.

- [7] R.P. Drake. Spike penetration in blast-wave-driven instabilities. *Astrophysical Journal*, 744(2):184–195, 2012.
- [8] SG Glendinning, J. Bolstad, DG Braun, MJ Edwards, WW Hsing, BF Lasinski, H. Louis, A. Miles, J. Moreno, TA Peyser, et al. Effect of shock proximity on richtmyer–meshkov growth. *Physics of Plasmas*, 10:1931, 2003.
- [9] J. Glimm and D.H. Sharp. Chaotic mixing as a renormalization-group fixed point. *Physical review letters*, 64(18):2137–2139, 1990.
- [10] MJ Grosskopf, RP Drake, CC Kuranz, AR Miles, JF Hansen, T. Plewa, N. Hearn, D. Arnett, and JC Wheeler. Modeling of multi-interface, diverging, hydrodynamic experiments for the national ignition facility. *Astrophysics and Space Science*, 322(1):57–63, 2009.
- [11] S.W. Haan, S.M. Pollaine, J.D. Lindl, L.J. Suter, R.L. Berger, L.V. Powers, W.E. Alley, P.A. Amendt, J.A. Futterman, W.K. Levedahl, et al. Design and modeling of ignition targets for the national ignition facility. *Physics of Plasmas*, 2:2480, 1995.
- [12] I. Hachisu, T. Matsuda, K. Nomoto, and T. Shigeyama. Nonlinear growth of rayleigh-taylor instabilities and mixing in sn 1987a. *The Astrophysical Journal*, 358:L57–L61, 1990.
- [13] J. Hecht, U. Alon, and D. Shvarts. Potential flow models of rayleigh–taylor and richtmyer–meshkov bubble fronts. *Physics of fluids*, 6:4019, 1994.
- [14] C. Kuranz, H. S. Park, B. Remington, R. Drake, A. Miles, H. Robey, J. Kilkenny, C. Keane, D. Kalantar, C. Huntington, C. Krauland, E. Harding, M. Grosskopf, D. Marion, F. Doss, E. Myra, B. Maddox, B. Young, J. Kline, G. Kyrala, T. Plewa, J. Wheeler, W. Arnett, R. Wallace, E. Giraldez, and A. Nikroo. Astrophysically relevant radiation hydrodynamics experiment at the national ignition facility. *Astrophysics and Space Science*, 336:207–211, 2011. 10.1007/s10509-011-0679-9.
- [15] M. Lafon, X. Ribeyre, and G. Schurtz. Gain curves and hydrodynamic modeling for shock ignition. *Physics of Plasmas*, 17:052704, 2010.
- [16] J.T. Larsen and S.M. Lane. Hyades—a plasma hydrodynamics code for dense plasma studies. *Journal of Quantitative Spectroscopy and Radiative Transfer*, 51(1-2):179–186, 1994.
- [17] E. E. Meshkov. Instability of the interface of two gases accelerated by a shock. *Fluid Dyn.*, 4:101, 1969.
- [18] A. R. Miles, D. G. Braun, M. J. Edwards, H. F. Robey, R. P. Drake, and D. R. Leibbrandt. Numerical simulation of supernova-relevant laser-driven hydro experiments on omega. *Physics Of Plasmas*, 11(7):3631–3645, 2004.

- [19] M. Morris. Astrophysics: The final plunge. *Nature*, 481(7379):32–33, 2012.
- [20] D. Oron, L. Arazi, D. Kartoon, A. Rikanati, U. Alon, and D. Shvarts. Dimensionality dependence of the rayleigh–taylor and richtmyer–meshkov instability late-time scaling laws. *Physics of Plasmas*, 8(6):2883–2889, 2001.
- [21] BA Remington, J. Kane, RP Drake, SG Glendinning, K. Estabrook, R. London, J. Castor, RJ Wallace, D. Arnett, E. Liang, et al. Supernova hydrodynamics experiments on the nova laser. *Physics of Plasmas*, 4(CONF-961102–), 1997.
- [22] R. D. Richtmyer. Taylor instability in shock acceleration of compressible fluids. *Commun. Pure Appl. Math*, 13:297, 1960.
- [23] VA Smalyuk, SX Hu, VN Goncharov, DD Meyerhofer, TC Sangster, D. Shvarts, C. Stoeckl, B. Yaakobi, JA Frenje, and RD Petrasso. Rayleigh-taylor growth stabilization in direct-drive plastic targets at laser intensities of  $1 \times 10^{15}$  w/cm<sup>2</sup>. *Physical review letters*, 101(2):25002, 2008.
- [24] J. W. Strutt (Lord Rayleigh). Investigation of the character of the equilibrium of an incompressible heavy fluid of variable density. *Scientific Papers*, 2:207–220, 1900.
- [25] G. I. Taylor. The instability of liquid surfaces when accelerated in a direction perpendicular to their planes. *Proc. Royal Soc. A*, 2:192–196, 1950.
- [26] D.L. Youngs. Numerical simulation of turbulent mixing by rayleigh-taylor instability. *Physica D: Nonlinear Phenomena*, 12(1):32–44, 1984.
- [27] Q. Zhang and S.I. Sohn. An analytical nonlinear theory of richtmyer-meshkov instability. *Physics Letters A*, 212(3):149–155, 1996.
- [28] Q. Zhang and S.I. Sohn. Nonlinear theory of unstable fluid mixing driven by shock wave. *Physics of Fluids*, 9:1106, 1997.